11-1-2008

# Morphology of the Dayside Ionosphere of Venus: Implications for Ion Outflows

Jane L. Fox
*Wright State University - Main Campus*, jane.fox@wright.edu

# Morphology of the dayside ionosphere of Venus: Implications for ion outflows

J. L. Fox[1]

Received 9 May 2008; revised 3 July 2008; accepted 1 August 2008; published 5 November 2008.

[1] The nightside ionosphere of Venus is formed mostly by day-to-night transport of ions below the ionopause, with a small contribution from precipitation of energetic electrons from the wake. This nightward flux of ions should result in dayside ionospheres that are characterized by smaller electron density scale heights at high altitudes than those that are characteristic of diffusive equilibrium. In order to determine both the maximum possible values of the upward fluxes and the upward fluxes implied by comparison of our computed ion and electron density profiles to measurements, we have constructed more than 60 models of the high solar activity Venus ionosphere for upward velocity boundary conditions ranging from 0 to $3 \times 10^5$ cm $s^{-1}$. We show that as the upward velocity at the top of the model is increased, the high-altitude densities of the atomic ions decrease, as do the total ion and electron densities. The maximum upward $O^+$ flux that we derive is $\sim 5.3 \times 10^8$ $cm^{-2}$ $s^{-1}$. By comparing our model electron or total ion density profiles to those from Pioneer Venus data, we have derived upward fluxes of $O^+$ that range from $1.8 \times 10^8$ to $2.5 \times 10^8$ $cm^{-2}$ $s^{-1}$ with an average of $2.1 \times 10^8$ $cm^{-2}$ $s^{-1}$. This value is roughly equal to estimates of the transterminator ion flux and to estimates of the downward fluxes of ions over the nightside. From this, we infer that the escape flux due to ion outflow is small. We conclude that the upward fluxes of ions that we have inferred from the morphology of the ionosphere contribute mostly to the day-to-night flow and to the formation of the nightside ionosphere and are much less than their source-limited values.

**Citation:** Fox, J. L. (2008), Morphology of the dayside ionosphere of Venus: Implications for ion outflows, *J. Geophys. Res.*, *113*, E11001, doi:10.1029/2008JE003182.

## 1. Introduction

[2] The presence of a nightside ionosphere on Venus was discovered by radio occultation measurements by the Mariner 5 spacecraft [e.g., *Kliore et al.*, 1967; *Mariner Stanford Group*, 1967], but its existence was puzzling in view of the long period of the Venus night, which lasts for 58 Earth days. Several mechanisms for production of the nightside ionosphere were initially proposed [cf. *McElroy and Strobel*, 1969]. Significant progress in elucidating its sources became possible only with the analysis of data from instruments on board the Soviet Venera 9 and 10 orbiters, and the US Pioneer Venus Orbiter (PVO). Beginning in 1975, the Venera orbiters carried out radio occultation experiments to determine the electron density profiles, and in situ plasma experiments, which showed the existence of fluxes of suprathermal electrons at high altitudes in the optical shadow of Venus [e.g., *Gringauz et al.*, 1977]. The PVO began in situ measurements in December 1978, and a suite of instruments provided data about the Venus thermosphere/ionosphere for nearly three diurnal cycles of 225 days each, at moderately high to high solar activity. Four instruments provided in situ information about the ion densities and velocities: the Orbiter Ion Mass Spectrometer (OIMS) measured individual thermal ion densities, and in superthermal mode, ions with energies in the range 9 to 16 eV [e.g., *Taylor et al.*, 1980]; the Orbiter Retarding Potential Analyzer (ORPA) provided data about the drift velocities and the number densities of $O^+$, $O_2^+$ and "mass 29" ions, which represents the sum of the densities of the molecular ions $N_2^+$, $CO^+$, and $NO^+$ [e.g., *Knudsen et al.*, 1980a, 1981]; the Orbiter Electron Temperature Probe (OETP) measured the electron densities and temperatures [e.g., *Brace et al.*, 1980]; the Orbiter Neutral Mass Spectrometer (ONMS) measured the densities of several neutral species [e.g., *Niemann et al.*, 1980], and, in ion mode, the densities of ions with energies greater than 36 eV [e.g., *Kasprzak et al.*, 1991]. In addition, the PV Orbiter Radio Occultation (ORO) experiment provided electron density profiles throughout the 14 years of the mission, which encompassed nearly the entire range of solar zenith angle (SZA) and solar activity (see, e.g., the reviews by *Kliore and Mullen* [1989], *Kliore* [1992], and *Fox and Kliore* [1997]).

[3] Dozens of papers have subsequently been written about the sources and characteristics of the nightside ionosphere of Venus, and it would be impossible to describe

[1]Department of Physics, Wright State University, Dayton, Ohio, USA.


0148-0227/08/2008JE003182

them all in detail. It is now generally recognized, however, that the nightside ionosphere is maintained mainly by day-to-night transport of ions, which are accelerated by the plasma pressure gradient force [e.g., *Taylor et al.*, 1980; *Knudsen et al.*, 1981; *Cravens et al.*, 1983; *Whitten et al.*, 1984; *Nagy et al.*, 1991]. A small and apparently variable source of ionization is due to the precipitation of some portion of the energetic electrons that were detected at high altitudes in the planetary wake both by the plasma experiments on the Venera 9 and 10 spacecraft at low solar activity [e.g., *Gringauz et al.*, 1977, 1979; *Breus et al.*, 1985], and by the RPA on PVO at high and moderate solar activity [e.g., *Knudsen et al.*, 1980b; *Spenner et al.*, 1981, 1996]. The energies of these electrons is of the order of tens of eV.

[4] *Knudsen and Miller* [1992] estimated that at high solar activity, up to 25% of the ions observed on the nightside could be produced by electron impact. The appearance of aurorally induced OI emissions at 1304 and 1356 Å on the nightside of Venus is evidence that at least some of the observed electrons precipitate into the nightside thermosphere. Using a simplified model for electron transport, *Fox and Stewart* [1991] concluded that 28% of the electron fluxes reported by *Knudsen and Miller* [1985] could produce the average OI 1356 Å intensity of 4 R. This fraction was later refined to 23% by *Fox et al.* [1992], who used a more accurate multistream electron transport code.

[5] Atomic ions, which, in general, have longer lifetimes than the molecular ions, have been observed to flow upward and nightward across the terminator, where they may converge and flow downward to produce a nightside ionosphere via reactions with the ambient neutral species [e.g., *Miller and Whitten*, 1991]. The major atomic ion is observed to be $O^+$, and it reacts efficiently with the $CO_2$ in the nightside thermosphere to produce $O_2^+$:

$$O^+ + CO_2 \rightarrow O_2^+ + CO. \quad (1)$$

Subsequently, the $O_2^+$ may react with N to produce $NO^+$:

$$O_2^+ + N \rightarrow NO^+ + O. \quad (2)$$

[6] In the nightside predawn ''hydrogen bulge'' region, which extends roughly from 2200 to 0400 h local time, the densities of H are inferred to be enhanced over the dayside values by factors of up to 400 [e.g., *Brinton et al.*, 1980; *Taylor et al.*, 1984, 1985; *Grebowsky et al.*, 1995]. In this region, the near resonant charge transfer reaction of $O^+$ with H

$$O^+ + H \rightarrow H^+ + O \quad (3)$$

produces a bulge in the $H^+$ densities also.

[7] There is presumably some small contribution owing to transport of atomic ions other than $O^+$ from the dayside to the nightside, and subsequent reactions such as

$$N^+ + CO_2 \rightarrow CO_2^+ + N, \quad (4)$$

$$N^+ + CO_2 \rightarrow CO^+ + NO, \quad (5)$$

$$N^+ + CO \rightarrow NO^+ + C, \quad (6)$$

$$N^+ + CO \rightarrow CO^+ + N, \quad (7)$$

and

$$C^+ + CO_2 \rightarrow CO^+ + CO. \quad (8)$$

The charge transfer reactions of $He^+$ are mostly dissociative, and include, for example,

$$He^+ + CO_2 \rightarrow CO^+ + O + He, \quad (9)$$

$$He^+ + CO_2 \rightarrow O^+ + CO + He, \quad (10)$$

$$He^+ + CO \rightarrow C^+ + O + He, \quad (11)$$

and

$$He^+ + N_2 \rightarrow N^+ + N + He. \quad (12)$$

Some nondissociative reactions, such as

$$He^+ + N_2 \rightarrow N_2^+ + He, \quad (13)$$

and

$$He^+ + CO_2 \rightarrow CO_2^+ + He, \quad (14)$$

also occur. Thus, the nightside ionosphere is observed to be made up of the same ions as the dayside ionosphere, albeit with different relative densities [*Taylor et al.*, 1980].

[8] The nightward flow pattern of ions is observed not to be symmetrical about the Venus-Sun line, but appears to be influenced by the neutral superrotation, with regions of divergence and convergence displaced from noon and midnight toward the dawn terminator [e.g., *Miller and Whitten*, 1991]. It was originally thought that the nightward flow was ''shut off'' at low solar activity, but *Brannon et al.* [1993] and *Dobe et al.* [1995] showed that nightward transport of ions is the most important source of the nightside ionosphere even at moderately low solar activity, which prevailed during the reentry period of the PV spacecraft in 1992 [cf. *Fox and Kliore*, 1997].

[9] Just as for Mars [e.g., *Chen et al.*, 1978; *Shinagawa and Cravens*, 1989; *Fox*, 1993, 1997], the presence of upward and nightward flowing ions should affect the dayside ion and electron density profiles, reducing the scale heights near and above the photochemical equilibrium (PCE) boundary. In the PCE region, the direct and chemical production rates of ions are approximately equal to their chemical loss rates. *Brace et al.* [1982a] had previously suggested that altitude profiles of $n_e$ should be ''eroded'', with scale heights that are less than that for diffusive equilibrium below the ionopause, and such ionospheres

were reported by *Brace et al.* [1980] from PV OETP data. These eroded ionospheres may be modeled in one dimension by imposing either upward flux or upward velocity boundary conditions on the ions at the top of the models.

[10] We construct here a number of models of the high solar activity Venus ionosphere for various upward velocity boundary conditions on all the ions, except for $O^{++}$, which is assumed to be in PCE, and we compute the implied fluxes of various ions. We show that initially, as the velocity is increased, the derived upward fluxes increase nearly linearly. Eventually, however, further increases in the upward velocity lead to compensating decreases in the topside ion densities, and the inferred upward fluxes of the ions begin to level off. For upward velocities of the order of $3 \times 10^5$ cm $s^{-1}$, the limiting value of the upward flux of most of the atomic ions on the dayside is reached.

[11] The limiting values of the upward fluxes of the ions averaged over the dayside is also an upper limit to the converging downward fluxes of ions over the nightside of the planet. We investigate here whether the limiting fluxes are attained, or if smaller values are implied by the data. It has been suggested that upward and nightward flows of ions at lower altitude may converge and flow downward on the nightside, and that at higher altitudes these ions may escape from the gravitational field of the planet [e.g., *Knudsen et al.*, 1980a].

## 2. Model

[12] We have here constructed models of the Venus thermosphere/ionosphere that are similar to those of *Fox and Sung* [2001], but which have been updated with revised rate coefficients, cross sections, and radiative lifetimes as described by *Fox* [2003, 2004, 2007], and by *Fox and Yeager* [2006]. Diffusion and eddy diffusion are included for the neutrals, and ambipolar diffusion is included for the ions. The background neutral densities of the major species $CO_2$, O, CO, He, N, and $N_2$, were adopted from the empirical global VTS3 models that were developed by *Hedin et al.* [1983]. We have included 6 additional species, including Ar, C, NO, He, H and $H_2$ for a total of 12 background species. We compute the density profiles for 14 ions, including $O_2^+$, $CO_2^+$, $N_2^+$, $Ar^+$, $O^+(^4S)$, $O^+(^2D)$, $O^+(^2P)$, $CO^+$, $C^+$, $N^+$, $NO^+$, $O^{++}$, $He^+$, and $H^+$, and 9 neutral species, including NO, $N(^4S)$, $N(^2D)$, $N(^2P)$, C, $O(^1D)$, $O(^1S)$, H, and $H_2$. We confine our attention here to high solar activity, for which there is much more information about ion densities from in situ measurements, than for low solar activity.

[13] We have adopted here the Solar2000 (S2K) v2.22 99178 solar flux model from *Tobiska* [2004; also private communication, 2000]. The 99178 fluxes correspond to day 178 (27 June) of 1999, for which the value of $F_{10.7}$ adjusted to 1 AU was 214. The S2K v2.2x spectra are normalized to the measurements from the Solar EUV Experiment (SEE) on the Thermosphere Ionosphere Mesosphere Energetics and Dynamics (TIMED) spacecraft. The SEE instrument has measured solar irradiances in the range 1 to 1940 Å in 10 Å intervals from 2002 to the present [e.g., *Woods et al.*, 2005] (see also the instrument Web site at http://lasp.colorado.edu/see). The format of the solar flux model that we use is that first proposed by *Hinteregger et al.* [1981, also private communication, 1979], in which the continuum fluxes are given in 1 Å intervals, and the strong solar lines are assumed to be delta functions at their central wavelengths, for a total of more than 1800 lines from 18 to 2000 Å. For harder X rays below 18 Å we adopt the solar fluxes from *Ayres* [1997; also private communication, 1996]. It should be noted that the use of the S2K v2.22 solar fluxes in ionospheric models has been shown to yield electron density peaks for Mars and Venus that are somewhat smaller than the experimentally determined peaks, and smaller than those in which the S2K 1.24 solar fluxes or the F79050N fluxes of Hinteregger are adopted [e.g., *Fox and Sung*, 2001; *Fox*, 2004, 2007; *Fox and Yeager*, 2006]. We have chosen a SZA of 60° to represent a dayside average model.

[14] We begin with the construction of a model for high solar activity of the dayside ion and electron density profiles with zero velocity upper boundary conditions. The top boundary of the model is assumed to be at 400 km. We then construct models in which upward velocity boundary conditions at the tops of the models are imposed. These velocities range from 0 to $3.0 \times 10^5$ cm $s^{-1}$ in small increments, for a total of more than 60 models. For each model with prescribed upward velocity boundary conditions, we predict the ion density profiles. We compute the upward fluxes of ions by multiplying the ion velocities by the ion densities at the tops of the models. By comparing the computed electron or total ion density profiles to the averaged profiles obtained from measurements by the PV ORO, the ORPA, and the OETP, we can estimate the implied upward fluxes.

[15] These inferred upward fluxes can also be compared to the estimated values for the transterminator fluxes of ions [e.g., *Knudsen and Miller*, 1992; *Brace et al.*, 1995]; to the downward fluxes of ions on the nightside [e.g., *Brannon et al.*, 1993; *Brannon and Fox*, 1994]; to the loss rates of molecular ions on the nightside due to dissociative recombination (DR) [e.g., *Knudsen et al.*, 1980a]; and to estimates of the ion escape rates, which will be discussed later.

[16] We also determine the maximum upward fluxes of ions that the high solar activity ionosphere can sustain, which are limited roughly by the production rate above the PCE boundary [cf. *Fox*, 1997]. This source-limited flux is fundamentally different from the diffusion controlled escape flux of a light neutral species that is transported by diffusion from the lower atmosphere across the homopause to the exobase in a planetary atmosphere. We show that upward fluxes implied by the data are significantly smaller than the maximum fluxes that the ionospheres can sustain.

## 3. Electron and Ion Density Profiles

[17] In Figure 1, we show the computed ion and electron density profiles for the high solar activity ionosphere for four values of the upward ion velocity boundary conditions: 0, $2 \times 10^4$, $1 \times 10^5$, and $2 \times 10^5$ cm $s^{-1}$. In these plots the density profiles labeled $O^+$ are the sum of the densities of the ground $O^+(^4S)$ state and those of the excited $O^+(^2D)$ and $O^+(^2P)$ states. It is clear from these plots that the magnitude of the upward velocity boundary conditions makes little difference in the ion densities below about 180 km. The density profiles of $O^+$, other atomic ions, and electrons,

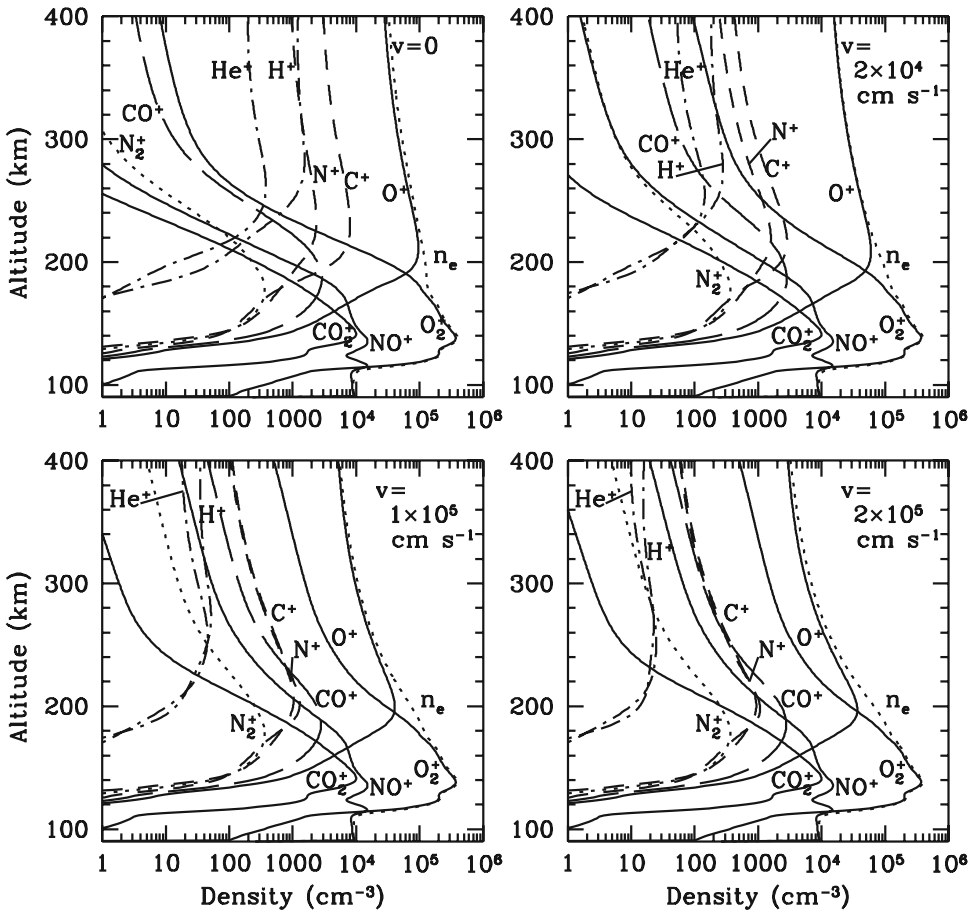


**Figure 1.** Computed density profiles of the major ions in the Venus ionosphere for four values of the upward velocity imposed at the top of the model: 0, $2 \times 10^4$, $1 \times 10^5$, and $2 \times 10^5$ cm s$^{-1}$. The curve labeled $O^+$ represents the sum of the $O^+(^4S)$, $O^+(^2D)$, and $O^+(^2P)$ densities. The topside atomic ion densities are shown to decrease, and the molecular ion densities increase as the upward velocity increases.

however, exhibit obvious monotonic decreases near and above about 200 km. The decrease in the density of $H^+$ is amplified over that because of its upward flux by the reduced rate of production by charge transfer from $O^+$ (reaction (3)), which is the main source of $H^+$ above 160 km.

[18] The high-altitude $O_2^+$ and $NO^+$ density profiles show a large increase as the upward velocity boundary condition increases. This behavior is due to the decrease in the rate of loss of the ions by the DR reactions

$$O_2^+ + e \rightarrow O + O, \tag{15}$$

and

$$NO^+ + e \rightarrow N + O, \tag{16}$$

as the electron density decreases. Reaction (15) is the major loss process for $O_2^+$ above ~120 km. Since NO has the lowest ionization potential among all the thermospheric species, reaction (16) is the only chemical loss mechanism for $NO^+$ over the entire altitude range of the model.

[19] At higher altitudes, DR becomes the major loss process for all the other molecular ions in our model as well, and their densities thus also increase as the upward velocity imposed at the top of the model increases. For example, for the zero upward velocity boundary condition model, DR of $CO_2^+$

$$CO_2^+ + e \rightarrow CO + O, \tag{17}$$

and $CO^+$

$$CO^+ + e \rightarrow C + O, \tag{18}$$

are the major loss processes for the ions above ~245 and ~230 km, respectively. The DR reaction

$$N_2^+ + e \rightarrow N + N, \tag{19}$$

is the major loss process for $N_2^+$ above ~220 km.

[20] The computed upward fluxes for various species at the tops of the high solar activity model as a function of upward velocities in the range 0 to $3 \times 10^5$ cm s$^{-1}$ are shown in Figure 2. In Figure 2 (top), we present the upward fluxes for the ions $O^+(^4S)$, "total $O^+$", and $O_2^+$. Total $O^+$ refers to the sum of $O^+(^4S)$ and $O^+(^2D)$. In the altitude range of interest here, $O^+(^2P)$ radiates or reacts faster than it can be transported.

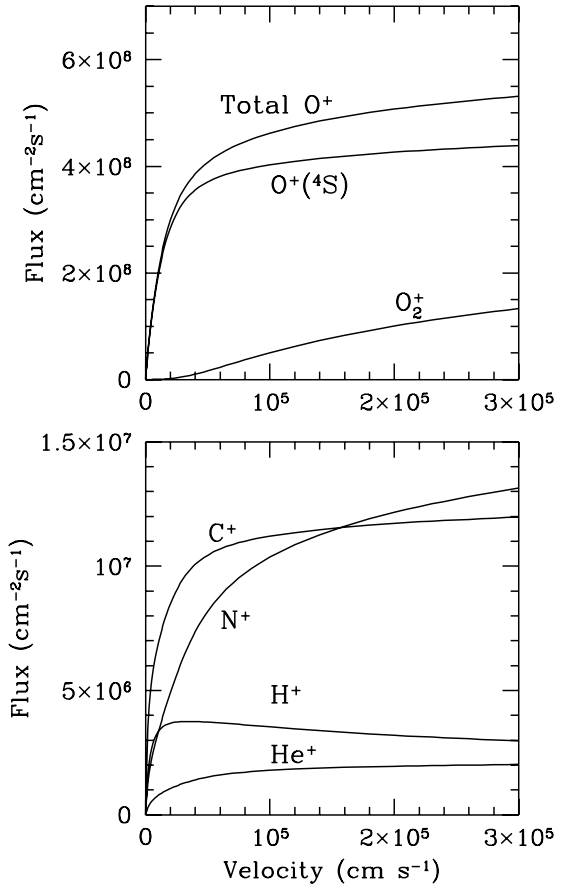


**Figure 2.** Computed fluxes of various atomic ions as a function of upward velocity at the tops of the models. The upward velocities range from 0 to $3 \times 10^5$ cm s$^{-1}$. (top) Fluxes of $O^+(^4S)$ and total $O^+$, which is the sum of $O^+(^4S)$ and $O^+(^2D)$ and $O_2^+$. (bottom) Fluxes of $C^+$, $N^+$, $H^+$, and $He^+$. Note the different flux scales for Figure 2 (top) and Figure 2 (bottom).

[21] For small upward velocities, the ion densities at the top of the model do not change appreciably. Thus, for velocities less than about $2 \times 10^4$ cm s$^{-1}$, the $O^+$ fluxes can be seen to increase nearly linearly as the velocities increase. For upward velocities larger than $\sim 4 \times 10^4$ cm s$^{-1}$, however, the $O^+$ densities at the top of the model begin to decrease as the upward velocities increase. Eventually, the corresponding upward fluxes increase more slowly until they reach a nearly constant value. The upward fluxes for $O^+$ do not increase significantly beyond a velocity of $\sim 2.5 \times 10^5$ cm$^{-2}$. Figure 2 shows that the practical upper limit to the upward flux of $O^+$ is $\sim 5.3 \times 10^8$ cm$^{-2}$ s$^{-1}$, and the upper limit to the total atomic ion flux is $\sim 5.6 \times 10^8$ cm$^{-2}$ s$^{-1}$.

[22] In addition, as the upward velocity increases, the upward flux of $O_2^+$ begins to increase, and it appears that for upward velocities greater than $\sim 2 \times 10^5$ cm s$^{-1}$, the upward fluxes of $O_2^+$ itself may become important. This behavior is a result of the large increases in the high-altitude densities of $O_2^+$ that occur as the electron densities, and thus the rate of loss of $O_2^+$ by the DR reaction (15) decreases. The other molecular ions exhibit similar behavior. We will show later, however, that for the average upward fluxes of atomic ions that we derive, the fluxes of molecular ions are negligible.

[23] Figure 2 (bottom) shows the upward fluxes as a function of velocities for the minor atomic ions $C^+$, $N^+$, $H^+$, and $He^+$. The scale for the fluxes of these ions are expanded, and it is apparent that the fluxes of the minor ions constitute a small component of the total ion fluxes. We also note here that there is no a priori reason to believe that all the atomic ions should reach their maximum upward flux at the same upward velocity as $O^+$, except for those species whose densities are determined largely by the $O^+$ density.

[24] The flux of $H^+$ is seen to maximize for a velocity of $3.5 \times 10^4$ cm s$^{-1}$ at about $3.8 \times 10^6$ cm$^{-2}$ s$^{-1}$ and then decrease slowly to a value of about $\sim 3 \times 10^6$ cm$^{-2}$ s$^{-1}$ as the velocity increases to a value of $3 \times 10^5$ cm s$^{-1}$. The appearance of a maximum is due the importance of the charge transfer reaction from $O^+$ to H (reaction (3)), which is the main source of $H^+$ in this altitude region, exceeding photoionization and electron impact ionization of H by 2 orders of magnitude. The rate of this reaction at high altitude decreases as the densities of $O^+$ decrease. Although the reverse of reaction (3)

$$H^+ + O \rightarrow O^+ + H \tag{20}$$

also occurs, the specific loss rate of $H^+$ in this reaction is nearly constant, since we assume here that the densities of O in the background model are fixed. Reaction (3) has a negligible effect on the $O^+$ density, for which other loss processes dominate.

[25] The $C^+$ fluxes reach maximum values of about $1.2 \times 10^7$ cm$^{-2}$ s$^{-1}$ at the maximum upward velocity of $3 \times 10^5$ cm$^{-2}$. Our model suggests that this behavior of the upward flux versus upward velocity is similar to that of $O^+$ because the major source of $C^+$ is charge transfer from $O^+$ to C:

$$O^+ + C \rightarrow O + C^+ \tag{21}$$

above 190 km.

[26] On the other hand, the $N^+$ fluxes increase monotonically from 0 to $\sim 1.3 \times 10^7$ cm$^{-2}$ s$^{-1}$ as the upward velocities increase from 0 to $3.0 \times 10^5$ cm s$^{-1}$. It is clear from Figure 2 that although the $N^+$ fluxes appear to "turn over" at about $10^5$ cm s$^{-1}$, the maximum flux is not reached for the maximum upward velocity in our models. Since the charge transfer reaction from $O^+$ to N is endothermic by 0.93 eV, the $N^+$ density does not depend on that of $O^+$, except for the increase of its diffusion coefficient as the total ion density decreases.

[27] The shape of the curves do not completely flatten out as the velocities in our models increase because, as the upward fluxes increase, the PCE boundaries decrease. Table 1 shows the PCE boundaries for three models, those for which the upward velocity boundary conditions are 0, $1 \times 10^5$ and $2.5 \times 10^5$ cm s$^{-1}$. These boundaries are located approximately where the lifetime against transport of an ion by diffusion, $\tau_D$, is equal to that due to chemical loss, $\tau_c$. $\tau_D$ is given approximately by the expression $H^2/D$, where $D$ is the diffusion coefficient for the ion and $H$ is the atmospheric

**Table 1.** Model Photochemical Equilibrium Boundaries for Three Upward Velocity Boundary Conditions[a]

| | Velocity (cm $s^{-1}$) | | |
|---|---|---|---|
| Species | 0 | $1.0 \times 10^5$ | $2.5 \times 10^5$ |
| $O^+$ | 203 | 203 | 202 |
| $O^+(^2D)$ | 247 | 227 | 225 |
| $C^+$ | 207 | 204 | 204 |
| $N^+$ | 222 | 215 | 214 |
| $H^+$ | 253 | 238 | 235 |
| $He^+$ | 230 | 223 | 221 |
| $O_2^+$ | 262 | 216 | 211 |
| $CO^+$ | 278 | 243 | 238 |
| $NO^+$ | 289 | 234 | 226 |
| $N_2^+$ | >400 | 269 | 255 |
| $CO_2^+$ | 287 | 250 | 245 |

[a]Units are km.

neutral scale height. The lifetime against loss by chemical reactions $\tau_c$ is the inverse of the specific loss rate $\mathcal{L}$, where

$$\mathcal{L} = \sum_i k_i n_X. \quad (22)$$

In this expression, $k_i$ is the $i$th rate coefficient for the reaction of ion with a species X, whose number density is given by $n_X$. For $O^+(^2D)$ we also include in this expression the Einstein A factor for radiation to $O^+(^4S)$, which leads to emission in the 3729, 3726 Å doublet. The transition probability for this emission is small, however, and has been reported recently as $8.199 \times 10^{-5}$ [*Froese-Fischer and Tachiev*, 2004]. It should be noted that the location of the PCE boundary is only an approximation. In fact, the major loss process for ions changes gradually from chemistry to transport by diffusion.

[28] The PCE boundaries for all ions are observed to decrease as the upward flux increases, and the computed decrease from 0 to $1 \times 10^5$ cm $s^{-1}$ is much larger than that from $1 \times 10^5$ to $2.5 \times 10^5$ cm $s^{-1}$. For atomic ions, the depression in the PCE boundary is largely due to the increase in the diffusion coefficients (and thus decreases in the diffusion lifetime) as the ion densities decrease. For the atomic ions the PCE boundary thus appears to fall moderately as the upward velocities increase. For the molecular ions, the chemical lifetimes also increase as the upward velocity boundary condition increases, owing to the decrease in the rates of DR reactions that destroy them as the ambient electron density decreases. These processes should both lead to lower PCE boundaries for the molecular ions, and, in fact, the altitudes of the model PCE boundaries are seen to decrease dramatically. In addition, as the PCE boundary is driven down, the production rate of ions available for transport increases. This effect explains the small continuing increase in the upward fluxes for some of the ions at high values of the upward velocities.

[29] The upper limit to the $O^+$ ion fluxes of $\sim 5.3 \times 10^8$ $cm^{-2}$ $s^{-1}$, is larger than the previously determined upper limit of $3.2 \times 10^8$ $cm^{-2}$ $s^{-1}$ [*Fox*, 1992]. The latter value was obtained, however, using upward flux boundary conditions in the model, rather than the more stable upward velocity boundary conditions. The flattening out of the upward fluxes of $O^+$ as a function of upward velocity in Figure 2 shows, however, that the upper limit that we have derived here is credible. It is noteworthy that *Fox* [1992] showed that when downward fluxes of $O^+$ of $\sim 3.2 \times 10^8$ $cm^{-2}$ $s^{-1}$ were imposed on a model of the nightside ionosphere, the resulting peak density of $O_2^+$ of $4 \times 10^4$ $cm^{-3}$ reproduced the maximum nightside electron densities measured by the PV ORO [*Kliore et al.*, 1991]. *Brace et al.* [1982a] determined what they called a "diffusion-limited" flux of $O^+$ of $\sim 2.5 \times 10^8$ $cm^{-2}$ $s^{-1}$, assuming that the $O^+$ ions were flowing through a stationary ionosphere of $O_2^+$ ions. We assume, however, that all the ions are flowing at the same speed through a stationary neutral atmosphere. Both assumptions contain inadequacies. In fact, some of the neutral species are probably dragged along by the ions, and the ion velocities probably differ from each other by values of the order of m $s^{-1}$.

## 4. Upward Fluxes of Ions Derived From Data

[30] We now use measured dayside average ion and electron density profiles to compare to the characteristics of our models in order to determine the upward ion fluxes implied by the data. Figure 3 shows a plot of the computed ratio of the electron number densities at 300 km to the peak value of our models of $3.95 \times 10^5$ $cm^{-3}$ near 138 km, as a function of upward flux. It is apparent that the ratio decreases slowly for small upward fluxes but decreases more rapidly for fluxes that are larger than $\sim 5 \times 10^7$ $cm^{-2}$ $s^{-1}$.

[31] First we consider the averaged PV ORO profiles presented by *Kliore and Luhmann* [1991], which are reproduced in Figure 4. The high solar activity profile is the average of six profiles between 60° and 70° SZA that were obtained during 1980. The ratio of the peak electron density to that at 300 km is about 0.083, and implies a total $O^+$ ion upward flux of $\sim 2.5 \times 10^8$ $cm^{-2}$ $s^{-1}$.

[32] The ion densities measured by the ORPA over 2 Earth years at solar maximum for a SZA range of 65 ± 5° are shown in Figure 5 [*Miller et al.*, 1984]. Since these data did not extend down to the electron density peak, we used the ratio of the total ion density at 300 km to those at

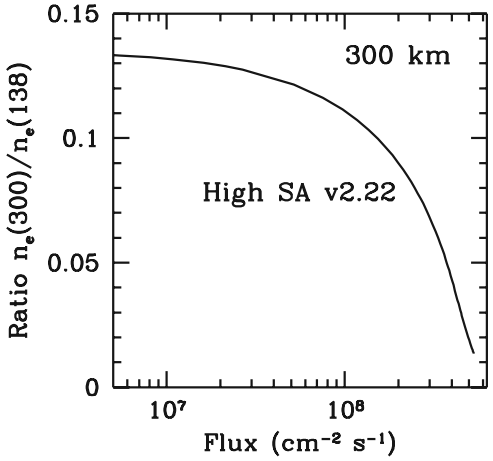


**Figure 3.** Computed ratio of the electron number density at 300 km to that at the ion peak, near 138 km, as a function of total upward fluxes of $O^+$ at the top of the model from $5 \times 10^6$ to $5.3 \times 10^8$ $cm^{-2}$ $s^{-1}$.

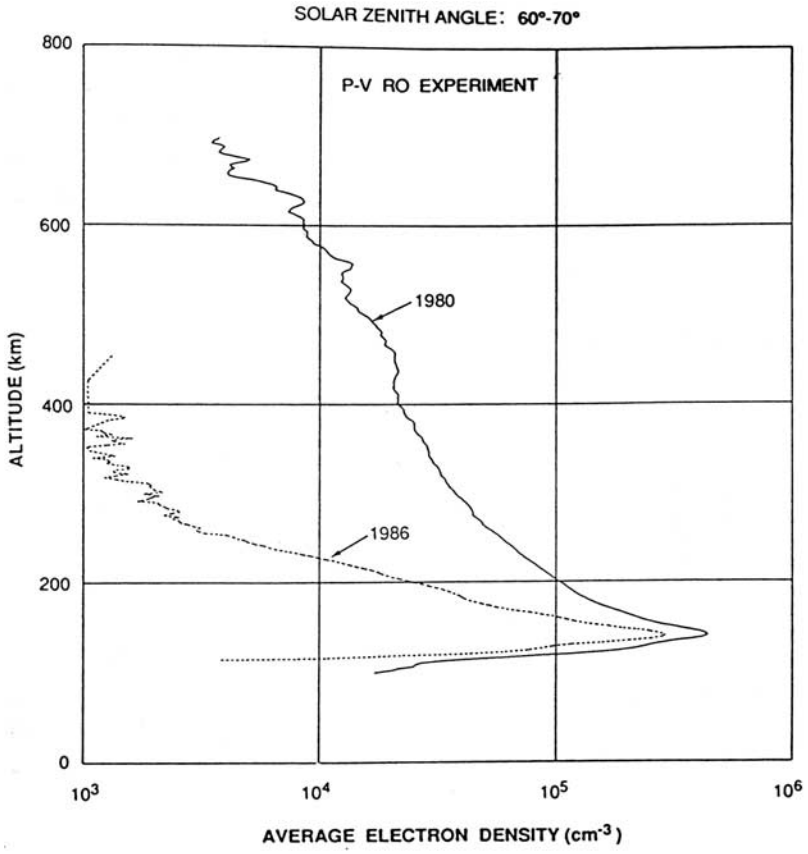


**Figure 4.** Average of 6 and 10 electron density profiles derived from Pioneer Venus (PV) Orbiter radio occultation profiles recorded between 60° and 70° solar zenith angle during high and low solar activities, respectively. From *Kliore and Luhmann* [1991].

150 km in our model ($2.73 \times 10^5$ cm$^{-3}$) to derive an upward ion flux of $\sim 1.8 \times 10^8$ cm$^{-2}$ s$^{-1}$.

[33] Errors inherent in this method of determining the implied upward flux, include locating the peak in the averaged PV ORO and ORPA data, which may differ slightly from our model peak height of 138 km, and from determining the densities by digitizing the profiles in Figures 4 and 5, for which the original data are not available. In addition, these fluxes may be slight overestimates because both experimental profiles pertained to averages over the solar zenith angle range 60° to 70°, whereas our model is for 60° SZA.

[34] Finally, we examine the revised empirical models of electron density derived from PV OETP data by *Theis et al.* [1984] for the first several years at high solar activity. Using these measurements, Theis et al. presented models that represent averages of electron densities at various altitudes and solar zenith angles. In these models the data were fit to error functions and exponentials rather than to spherical harmonics, and were considered to be better fits to the electron density profiles than those of *Theis et al.* [1980], especially near the terminators. From Table 3 of *Theis et al.* [1984] we choose the model for 60° SZA dusk, and use the ratio of the model density at 300 km to that at 150 km to derive an upward $O^+$ flux of $\sim 1.9 \times 10^8$ cm$^{-2}$ s$^{-1}$.

[35] The upward $O^+$ fluxes derived from high solar activity PVO data thus are in the range $(1.8-2.5) \times 10^8$ cm$^{-2}$ s$^{-1}$, and the average value is $\sim(2.1 \pm 0.4) \times 10^8$ cm$^{-2}$ s$^{-1}$. These implied $O^+$ fluxes are much less than our computed upper limit of $\sim 5.3 \times 10^8$ cm$^{-2}$ s$^{-1}$. In Table 2, we present the implied upward fluxes for several ions, as well as those of $O^+$, along with the computed maximum fluxes. We can compare the fluxes in Table 2 to the values of the integrated $O^+$ and total ion production rates above 200 km of $3.4 \times 10^8$ and $4.7 \times 10^8$ cm$^{-2}$ s$^{-1}$, respectively. These values are within a factor of $\sim 1.5$ of the maximum fluxes derived from the model.

## 5. Transterminator Fluxes

[36] *Knudsen et al.* [1981] showed that the $O^+$ ions in the vicinity of the terminator had antisunward components of velocities of 2–3 km s$^{-1}$, and were accelerated nightward by the plasma pressure gradient force. Various investigators have estimated the values of the transterminator fluxes of atomic ions, which have been assumed to be mostly $O^+$. We now compare our derived upward fluxes to the estimated values of the transterminator ion fluxes.

[37] Using early PVO RPA data near the terminators *Knudsen et al.* [1980a] derived a hemispheric average value of $3 \times 10^8$ cm$^{-2}$ s$^{-1}$ for the transterminator flux, referred to the surface. *Spenner et al.* [1981] revised the estimate to $(1-2) \times 10^8$ cm$^{-2}$ s$^{-1}$, which represents a total transterminator transport rate of $(2.3-4.6) \times 10^{26}$ s$^{-1}$. *Knudsen and Miller*

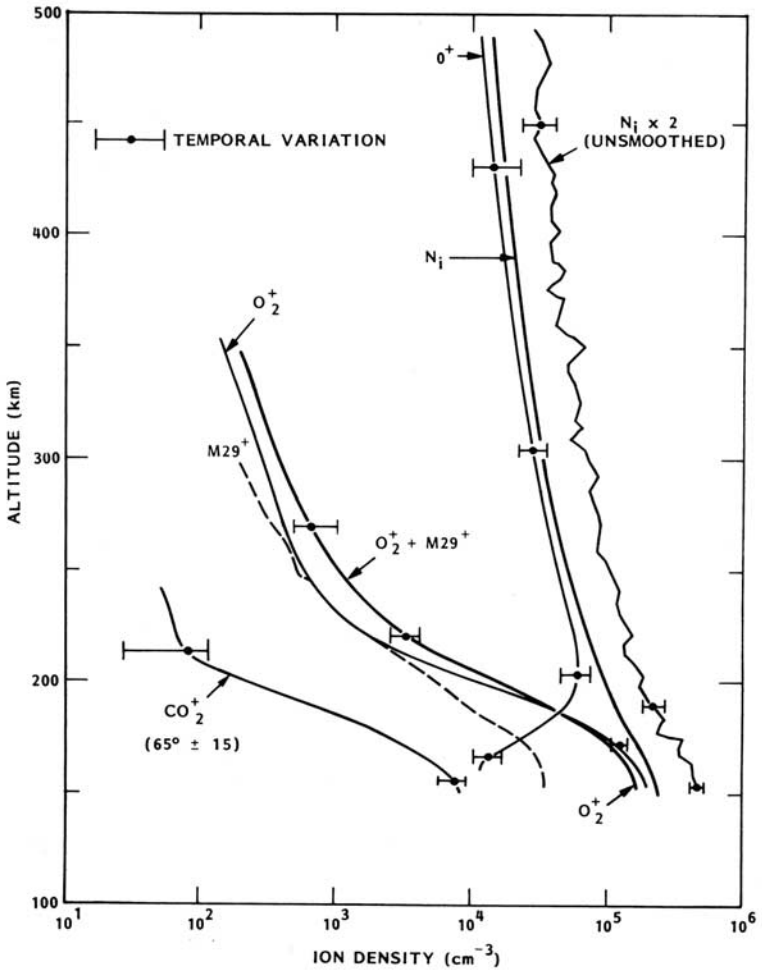


**Figure 5.** Smoothed median ion density profiles derived from all the Orbiter Retarding Potential Analyzer data in the interval 65 ± 5°. The total ion density is derived separately from the individual ions. The curve labeled $N_i \times 2$ is not smoothed, and the error bars indicate standard deviations. We used the smoothed curve labeled $N_i$ in our analysis. Reprinted from *Miller et al.* [1984] with permission from Elsevier.

[1992] later used the PVO RPA data to determine the ion densities and drift velocities in an annulus across the terminator, and further refined the value to a hemispherically average flux of $\sim 2.2 \times 10^8$ cm$^{-2}$ s$^{-1}$ or a total nightward ion transport rate of $\sim 5 \times 10^{26}$ s$^{-1}$. *Brace et al.* [1995] used PV OETP densities of electrons measured in the terminator region, along with the ion velocities from the PV ORPA, and derived a transterminator flux equal to a hemispheric average of $2 \times 10^8$ cm$^{-2}$ s$^{-1}$. These recent values are very close to the derived upward fluxes of ions for our 60° SZA model.

## 6. Downward Fluxes of Ions Over the Nightside

[38] Atomic ions flowing downward over the nightside of Venus react with the ambient neutrals to produce molecular ions in reactions such as those shown in equations (1)–(14). These molecular ions, after possible transformations, are ultimately destroyed in DR reactions, such as those enumerated in equations (15)–(19). Insofar as the loss rates of these ions by DR is equal to their production rates, that is,

**Table 2.** Computed Maximum and Inferred Upward Fluxes for Our 60° Solar Zenith Angle Models and Integrated Rates Over the Dayside Hemisphere

| Species | Maximum Flux (cm$^{-2}$ s$^{-1}$) | Inferred Flux (cm$^{-2}$ s$^{-1}$) | Integrated Rate (s$^{-1}$)[a] |
|---|---|---|---|
| $O^+$ | $4.4 \times 10^8$ | $2.0 \times 10^8$ | $4.6 \times 10^{26}$ |
| $O^+(^2D)$ | $9.2 \times 10^7$ | $7.5 \times 10^6$ | $1.7 \times 10^{25}$ |
| $C^+$ | $1.2 \times 10^7$ | $7.0 \times 10^6$ | $1.6 \times 10^{25}$ |
| $N^+$ | $1.3 \times 10^7$ | $3.5 \times 10^6$ | $8.0 \times 10^{24}$ |
| $H^+$ | $3.0 \times 10^6$ | $3.4 \times 10^6$ | $7.8 \times 10^{24}$ |
| $He^+$ | $2.0 \times 10^6$ | $8.1 \times 10^5$ | $1.9 \times 10^{24}$ |
| $O_2^+$ | $1.3 \times 10^8$ | $4.5 \times 10^5$ | $1.0 \times 10^{24}$ |
| $CO^+$ | $1.1 \times 10^7$ | $1.2 \times 10^5$ | $2.7 \times 10^{23}$ |
| $N_2^+$ | $1.3 \times 10^6$ | $1.1 \times 10^4$ | $2.5 \times 10^{22}$ |
| $NO^+$ | $5.6 \times 10^6$ | $5.9 \times 10^3$ | $1.3 \times 10^{22}$ |
| $CO_2^+$ | $1.7 \times 10^5$ | $4.2 \times 10^2$ | $9.6 \times 10^{20}$ |

[a]Obtained by integrating the inferred fluxes over the hemispheric surface area. These values are meaningful only insofar as the computed upward fluxes for 60° solar zenith angle correspond to dayside averages.

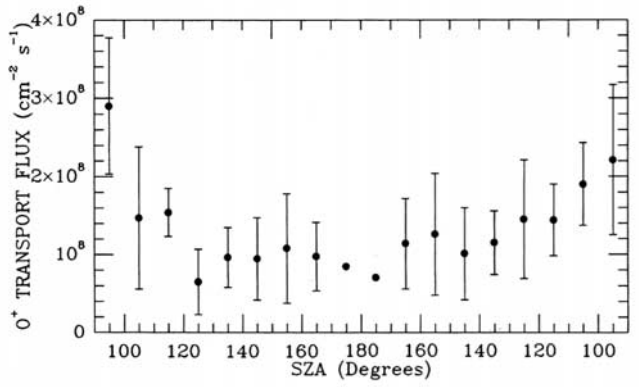


**Figure 6.** $O^+$ maximum density as measured by the PV Orbiter Ion Mass Spectrometer [e.g., *Taylor et al.*, 1980] as a function of solar zenith angle for (left) evening and (right) morning for 384 orbital segments from the first 2 years of the Pioneer Venus mission. The data are binned in 10° solar zenith angle intervals. The error bars are standard deviations. Reprinted from *Brannon and Fox* [1994] with permission from Elsevier.

assuming PCE, the column integrated loss rates are a measure of the downward fluxes of atomic ions over the nightside. *Knudsen et al.* [1980a] used RPA data for the nightside molecular ion densities, along with a DR rate coefficient of $8.75 \times 10^{-6}\ T_e^{-0.67}$ cm$^3$ s$^{-1}$ to estimate an altitude integrated molecular ion loss rate by DR averaged over the nightside of $2 \times 10^8$ cm$^{-2}$ s$^{-1}$.

[39] Using RPA data, *Knudsen et al.* [1980a] found that the ion velocity vectors near the terminator were directed antisunward and downward near the terminators, but were more horizontal at high altitudes. From measurements of $n_e$ [*Kliore et al.*, 1979] and $T_e$ [*Miller et al.*, 1980], they inferred that half of the loss of molecular ions by dissociative recombination occurs within 5° of the terminators, and therefore that "a large fraction of the $O^+$ transported across the terminators must be consumed close to it". Caution should be exercised here because the Venus ionosphere is sunlit to a solar zenith angle of 92–93° [e.g., *Whitten et al.*, 1982].

[40] *Brannon and Fox* [1994] modeled the nightside ionosphere of Mars, and derived the nearly linear relationships between the downward $O^+$ fluxes and the $O^+$ density maxima on the nightside as measured by the PV OIMS, as a function of local time and solar zenith angle. By comparing the modeled to the measured $O^+$ maxima, they constructed a map of the downward flux over the nightside as a function of SZA and hour angle. In Figure 6, we present one of the maps that shows the inferred average $O^+$ downward transport flux in 10° SZA bins with the dawn and dusk regions shown separately. The downward flux can be seen to maximize near the terminators, decrease with increasing SZA, then increase to a maxima near 150° in both the dawn and dusk sectors. There appear to be minima near the antisolar point. The structure of the binned data is similar to that exhibited by the PV ORO data at high solar activity, which shows a local minimum near 125° and a local maximum near 150° SZA [e.g., *Fox and Kliore*, 1997].

[41] Assuming that the behavior with solar zenith angle is latitude invariant, *Brannon and Fox* [1994] derived the average $O^+$ downward flux over the nightside as $1.5 \times 10^8$ cm$^{-2}$ s$^{-1}$. When the minor atomic ions were added, the total atomic ion flux was determined to be $1.7 \times 10^8$ cm$^{-2}$ s$^{-1}$. This estimate is somewhat smaller than the values of the transterminator fluxes, the nightside recombination rates, and the estimates of the upward fluxes of ions, but is within the probable uncertainties of all these quantities, which is of the order of ~35%.

## 7. Discussion

[42] In the high-altitude Venus ionosphere, atomic ions are observed to flow upward and nightward across the terminator. It is reasonable to assume that the ions that are flowing across the terminator at high altitudes either converge at large solar zenith angles or they may escape from the gravitational field of the planet. The value estimated by *Knudsen and Miller* [1992] for the nightward ion transport rate of $\sim 5 \times 10^{26}$ s$^{-1}$ (or a hemispherically averaged flux of $\sim 2.2 \times 10^8$ cm$^{-2}$ s$^{-1}$) is roughly equal to the nightside ionospheric recombination rate estimated by *Knudsen et al.* [1980a]. Therefore, *Knudsen and Miller* [1992] suggested that the loss of ions down the wake is smaller than that which converges and flows downward on the nightside by a factor of at least 5. *Knudsen* [1992] refined that value and estimated that the escape rate of ions was smaller by a factor of 10 than the transterminator fluxes.

[43] By comparison of our 60° solar zenith angle high solar activity model to three PV data sets, we have derived here upward fluxes of $O^+$ ions of $\sim 2.1 \times 10^8$ cm$^{-2}$ s$^{-1}$. Thus, the near equality between this value and the transterminator flux $2.2 \times 10^8$ cm$^{-2}$ s$^{-1}$ determined by *Knudsen and Miller* [1992], the hemispheric recombination rate estimated by *Knudsen et al.* [1980a] of $2 \times 10^8$ cm$^{-2}$ s$^{-1}$, and the downward flux of $O^+$ over the nightside derived by *Brannon and Fox* [1994] of $1.7 \times 10^8$ cm$^{-2}$ s$^{-1}$, suggests that there is little flux available for ion outflows, as *Knudsen* [1992] has suggested. Since, however, the accuracy of all these quantities is of the order of 35%, we conclude that escape by ion outflows either could be negligible, or could conceivably reach hemispherically average values of up to $\sim(4-5) \times 10^7$ cm$^{-2}$ s$^{-1}$, which corresponds to a total loss rate of $\sim(0.9-1.1) \times 10^{26}$ s$^{-1}$.

[44] The escape of ions from Venus has been discussed by various investigators, from modeling or measurements of specific ion acceleration mechanisms, and from observations of escaping ions. We summarize them below. We note here that in computations or measurements of processes relating to escape or upward, nightward, or downward flowing ions, the results are not reported in a uniform way. Sometimes local, hemispheric or global average fluxes are reported in units of cm$^{-2}$ s$^{-1}$ and sometimes the total rates of these processes integrated over a suitable surface area are reported in units of s$^{-1}$. Here we have modeled the upward fluxes of ions from the dayside, and we therefore report those fluxes in the units in which they are computed, cm$^{-2}$ s$^{-1}$. If, and only if, we assume that our computed fluxes represent averages over the dayside, we can multiply the fluxes by the dayside hemispheric surface area of Venus, and report total rates of upward flow, as shown in Table 2.

Therefore, for purposes of comparison of various processes involving computed or measured ion fluxes or rates, and where appropriate, we quote here both hemispheric average fluxes in units of $cm^{-2}\ s^{-1}$ and total rates with units of $s^{-1}$.

### 7.1. Pickup Ion Escape

[45] *Knudsen et al.* [1981] suggested that the heavy ions observed by the PV Orbiter Plasma Analyzer (OPA) flowing at solar wind speeds down the wake of the planet [e.g., *Mihalov et al.*, 1980] were pickup ions, rather than escaping ions arising from the day-to-night flows. Pickup ion escape is qualitatively different from the various loss processes that have been proposed to arise from bulk ion outflow, and does not cause the dayside ion density profiles to become eroded. Pickup ion escape occurs when atoms above the ionopause in the hot atom coronas of a planet are ionized by solar photoionization or impact ionization by solar wind electrons. An additional source for ionization of H and O is charge exchange with solar wind protons, which is resonant for H and near resonant for O (reaction (3)). Pickup ions may escape from the gravitational field of the planet if they are accelerated in an outward direction to the escape velocity by the convection ($-\mathbf{V} \times \mathbf{B}$) electric field of the solar wind [e.g., *Luhmann et al.*, 1992, 1995]. Evidence for pickup ions in the PV OPA and the Orbiter Magnetometer (OMAG) data was adduced by *Intriligator* [1989], who did a statistical analysis of the ion spectrum and the magnetic field data in the distant tail region of Venus. They observed "large" and "small" events, in which the $O^+$ pickup ion flux was found to be greater or less than $1.6 \times 10^7\ cm^{-2}\ s^{-1}\ sr^{-1}$, respectively.

[46] *Luhmann and Bauer* [1992] reviewed the escape rates of $O^+$ and O for Mars and Venus due to a number of processes and estimated a loss rate for the pickup ion process for Venus of $\sim 4 \times 10^{23}\ s^{-1}$ ($\sim 1.7 \times 10^5\ cm^{-2}\ s^{-1}$). *Terada et al.* [2004] used a 2-D global hybrid model to estimate the escape fluxes for four ion escape mechanisms, and found that the pickup ion escape rate varied with the solar wind dynamic pressure. They suggested a larger average value of $\sim 4 \times 10^{24}\ s^{-1}$ ($\sim 1.7 \times 10^6\ cm^{-2}\ s^{-1}$). *Kulikov et al.* [2006] studied $O^+$ pickup ion escape, as well as that due other processes, as function of time from present over the past 4.6 Gyr by applying a numerical test model. They determined an even larger current loss rate for pickup ions as $\sim 10^{25}\ s^{-1}$, equivalent to a hemispheric average of $\sim 4.3 \times 10^6\ cm^{-2}\ s^{-1}$.

[47] *Kallio et al.* [2006] used a 3-D quasi-neutral hybrid model with a 600 km grid spacing to model the nonthermal escape of ions due to the pickup process, including only photoionization of hot O as a source. They found that the particle source maximized at noon and decreased toward the terminator as cos(SZA). The computed $O^+$ total escape rate was similar to that of *Terada et al.* [2004], $\sim 4 \times 10^{24}\ s^{-1}$ ($\sim 1.7 \times 10^6\ cm^{-2}\ s^{-1}$). *Lammer et al.* [2006] also constructed a gas dynamic test particle model and derived the rates of escape due to several processes, including pickup ion escape, for which fairly large loss rates for $O^+$ and $H^+$ of $1.6 \times 10^{25}\ s^{-1}$ ($6.9 \times 10^6\ cm^{-2}\ s^{-1}$) and $1 \times 10^{25}\ s^{-1}$ ($4.3 \times 10^6\ cm^{-2}\ s^{-1}$), respectively, were predicted.

[48] *Luhmann et al.* [2007] emphasized that loss by pickup ion escape is enhanced greatly during times of high solar activity and during coronal mass ejections. They estimated the pickup ion escape rate at high solar activity to be of the order of $\sim 5 \times 10^{24}\ s^{-1}$ ($\sim 2.1 \times 10^6\ cm^{-2}\ s^{-1}$) but could increase by up to 2 orders of magnitude for 12–24 days per year. This would increase the pickup ion escape rate by factors of 3 to 7. *Luhmann et al.* [2007] suggested that escape fluxes during such periods may dominate the escape rate of ions at present and in past epochs.

[49] Thus, the estimates of the loss rate of $O^+$ due to pickup ion escape vary over nearly 2 orders of magnitude, but are small compared to the day-to-night fluxes, and therefore could be comparable to the potential escape processes due to ion outflows, which we discuss in section 7.2.

### 7.2. Escape due to Ion Outflows

[50] It is possible that some portion of the day-to-night ion fluxes that produce the "eroded ionospheres" that we model here, could result in escape by bulk ion outflow processes, although the total rate has been estimated to be small both here and by other investigators [e.g., *Knudsen et al.*, 1981; *Knudsen and Miller*, 1992; *Knudsen*, 1992]. Various bulk ion escape mechanisms that could arise from the day-to-night transport of ions have been studied by many investigators. We review here these escape processes, their proposed acceleration mechanisms, and the estimated loss rates or fluxes, where available.

[51] Beyond the terminator of Venus, at high altitudes, is the region that has become known as the ionotail. In this region, the Venus ionosphere becomes increasingly filamentary, forming comet-like tail rays and narrower filaments that extend several thousand km behind the planet. PV OETP data revealed wavelike structures and clouds of detached plasma near the terminators above the Venus ionopause on both the dayside and nightside of the planet [e.g., *Brace et al.*, 1982a]. The clouds could either be detached structures or filaments in various stages of detachment. It has been suggested that the clouds could be produced by the Kelvin-Helmholtz instability [e.g., *Pérez-de-Tejada*, 1980; *Terada et al.*, 2004]. The Kelvin-Helmholtz instability, which arises from the solar wind interaction with unmagnetized planets has been described by, for example, *Amerstorfer et al.* [2007]. *Biernat et al.* [2007] have modeled the solar wind flow past Venus, and they have found that the Kelvin-Helmholtz instability develops at the ionopause of Venus for a wide range of solar wind conditions.

[52] *Brace et al.* [1982a] estimated an upper limit to the total escape rate in the clouds of $\sim 7 \times 10^{26}\ s^{-1}$ ($3 \times 10^8\ cm^{-2}\ s^{-1}$). As pointed out previously, they suggested that this escape rate could be provided by a "diffusion limit" for $O^+$ diffusing through stationary $O_2^+$ of $2.5 \times 10^8\ cm^{-2}\ s^{-1}$. It is doubtful that the ion escape rate in clouds from this process is this large, however, since it exceeds estimates of the inferred upward or transterminator fluxes discussed above.

[53] More recently, *Lammer et al.* [2006] estimated a loss rate for ions in the plasma clouds observed by PV of $(0.5–1) \times 10^{25}\ s^{-1}$, equivalent to hemispheric average fluxes of $(2–4) \times 10^6\ cm^{-2}\ s^{-1}$. The range in the estimated escape rates for this process is partly due to the difficulty of determining the size and occurrence rate of the detached plasma clouds.

[54] Other estimates of ion loss due to the Kelvin-Helmholtz instability include those of *Terada et al.* [2002, 2004], who used a 2-D hybrid MHD model to determine the escape fluxes due to this process at the ionopause, which they proposed leads to a significant number of ions escaping from near and below the ionopause. An $O^+$ escape rate of $\sim 6 \times 10^{25}$ $s^{-1}$, equivalent to a hemispherically averaged flux of $2.5 \times 10^7$ $cm^{-2}$ $s^{-1}$, was predicted for times of low solar wind dynamic pressure. *Terada et al.* [2004] suggested, however, that during times of high solar wind dynamic pressure, the Kelvin-Helmholtz instability is suppressed, and there is no cloud removal taking place. The viscosity under these conditions is due to collisions between the neutrals and the ions at the ionopause. Terada et al., however, did not confine this escape mechanism to detached clouds, but suggested that the ion escape down the ionotail is also due to this process. They estimated an ion escape rate of $\sim 4 \times 10^{25}$ $s^{-1}$ ($1.3 \times 10^7$ $cm^{-2}$ $s^{-1}$) for conditions of high solar wind dynamic pressure.

[55] A detailed study of the ionotail with the OIMS, ONMS, OETP, and OMAG between 2000 and 2500 km showed that the magnetic fields in the rays are mostly radial or tailward, and that the outward flowing ions in the tail are composed mostly composed of $O^+$ with energies of 9–16 eV, those that are in the energy range that could be measured by the OIMS in superthermal mode [e.g., *Brace et al.*, 1987]. The dimensions of the rays are of order of $(1–3) \times 10^3$ km; the filaments have dimensions of tens of km across. The rays have ion densities of 50–500 $cm^{-3}$, whereas between the rays, in the troughs, the ion densities are of the order of 1–10 $cm^{-3}$. *Brace et al.* [1987] derived the escape fluxes from the plasma properties in the tail rays and filaments. They estimated that the $O^+$ escape flux down the tail was $\sim 5 \times 10^{25}$ $s^{-1}$, equivalent to a hemispherically averaged flux of $\sim 2 \times 10^7$ $cm^{-2}$ $s^{-1}$, and that the $H^+$ escape rate could be half that value.

[56] *Kasprzak et al.* [1987] used the ONMS in ion mode to detect ions with energies greater than ~36 eV near 2000 km and beyond 120° SZA. These superthermal $O^+$ ions represent only a small fraction of the ions in the tail region. Measurements by the OETP have shown that only about 1% of the ions in the tail are detected by the ONMS. Kasprzak et al. suggested that the $O^+$ density enhancements indicated tailward ion flow, but the fluxes of these very energetic ions was small, with average values on the order of $4 \times 10^4$ $cm^{-2}$ $s^{-1}$, and a maximum escape rate of $4 \times 10^6$ $cm^{-2}$ $s^{-1}$ was derived. In addition to $O^+$, the ONMS measured superthermal $He^+$, $N^+$, mass 28 ions ($N_2^+ + CO^+$), $NO^+$, and $O_2^+$ [e.g., *Kasprzak et al.*, 1991]. These ions could not be pickup ions from the hot atom coronas, but *Luhmann et al.* [1995] have proposed that loss of the heavier ionospheric ions could result from the penetration of the convection electric field into the high-altitude terminator ionosphere. Thus the acceleration mechanism for the heavy ions could be the similar to that of $O^+$ pickup ions.

[57] Structures known as "ionospheric holes" commonly appeared on the of the nightside of Venus, and were characterized by extreme plasma depletion above about 200 km, with electron densities that drop suddenly to less than 10 $cm^{-3}$, and in which the magnetic field is vertical and enhanced [*Brace et al.*, 1980, 1982b; *Grebowsky and Curtis*, 1981]. The holes are found in two broad regions north and south of the equator, and appear to have a lateral extent of ~600–800 km. These holes have been interpreted as regions in which ions flow outward from the ionosphere with high energies. *Grebowsky and Curtis* [1981] suggested that the plasma depletions were due to outward ion acceleration by parallel electric fields. They also suggested that electrons were accelerated downward in the holes to produce ionization in the thermosphere below 200 km. Grebowsky and Curtis did not, however, estimate the total loss rate of ions from these holes.

[58] *Hartle and Grebowsky* [1990] used ion composition measurements made by the PV OIMS in the holes and showed that the major ions $O^+$, $NO^+$, $O_2^+$, $H^+$, and $He^+$ flow upward along the axes of the holes. They derived flow speeds of the order of $1 \times 10^5$ cm $s^{-1}$ for $H^+$ and $He^+$, and somewhat smaller velocities for $O^+$, $O_2^+$ and $NO^+$, of the order of $1 \times 10^4$ cm $s^{-1}$, from the measurements. They suggested that the nightside holes were produced by a polar wind-like outflow, in which the ions are accelerated by the plasma pressure gradient force. They proposed that $H^+$ and $He^+$ ions are also buoyed up by the polarization electric fields and by thermal diffusion. The source of ions in the holes was uncertain, but was suggested to be the horizontally flowing plasma on the nightside. Hartle and Grebowsky proposed that the observed outward flowing $O_2^+$ could be produced chemically by reaction of downward flowing $O^+$ with $CO_2$ (reaction (1)), and possibly by energetic electron impact by the inward flowing electrons. The upward $O^+$ flux in the holes for the orbits considered was estimated to be of the order of $10^8$ $cm^{-2}$ $s^{-1}$. The total escape rate could not be estimated because of the uncertainty in the size and shape of the holes.

[59] *Donahue and Hartle* [1992] later suggested that the upward flow of $H^+$ and $D^+$ due to the polarization electric field could be responsible for escape of ions from the hydrogen bulge region as well as from the holes. *Hartle and Grebowsky* [1993] investigated flow characteristics of $H^+$ and $He^+$ at high solar activity in the region of the nightside ionosphere from midnight to 0200 h local time, where the densities of H, $H^+$, and $He^+$ are observed to maximize. They constructed averaged altitude profiles of $H^+$, and used the momentum equations to derive a planetary-averaged escape flux of $1.4 \times 10^7$ $cm^{-2}$ $s^{-1}$ at the ion exobase near 500 km, or a total escape rate of $7.5 \times 10^{25}$ $s^{-1}$. They found that the $H^+$ ions were accelerated outward to speeds of up to $1 \times 10^5$ cm $s^{-1}$, but the $O^+$ and $He^+$ density profiles indicated that these ions were flowing downward. The escape of $H^+$ is not limited by the day-to-night flow of $H^+$, since the $H^+$ ions in the bulge region on the nightside are produced mostly by charge transfer from the nightward flowing $O^+$ ions [e.g., *Grebowsky et al.*, 1995], and therefore could conceivably originate from the $O^+$ transterminator fluxes.

[60] *Hartle and Grebowsky* [1995] carried out similar studies in which they examined profiles of $H^+$ and $D^+$ on the Venus nightside from the PV OIMS measurements. They proposed in this study also that the altitude profiles of the ions indicate that they are flowing upward because of the polarization electric field, and more massive species, such as $He^+$, were found not to be accelerated outward by this mechanism. For the region between midnight and 0200 h local time, Hartle and Grebowsky estimated a

slightly larger total $H^+$ escape rate of $8.6 \times 10^{25}$ $s^{-1}$, equivalent to a hemispheric average escape flux for $H^+$ of $3.7 \times 10^7$ $cm^{-2}$ $s^{-1}$.

### 7.3. Measurements of Energetic Ions in the Solar Wind Cavity

[61] *Mihalov et al.* [1980] collected data from the PVO OPA, which was designed to measured the solar wind interaction with Venus. Measurements were made in the "plasma cavity," which is identified by a sharp decrease in proton flux about 10 $R_V$ downstream from the planet. The frequent episodic disappearances of magnetosheath plasma were accompanied by sporadic bursts of energetic ~4–8 keV ions, which were identified as $O^+$. The PVO made a series of passes through the solar wind in the wake of Venus at distances of 8–12 $R_V$ and made measurements of disappearing and reappearing plasma in the wake region. $O^+$ ions were detected in the cavity moving in the antisunward direction, with larger energies than those of the lighter ions, such as $H^+$. *Mihalov and Barnes* [1982] suggested that the high-energy ions were of ionospheric origin, comoving with the shocked solar wind.

[62] If the derived ion outflow were not intermittent, a total loss rate of $\sim 10^{25}$ $s^{-1}$ would be inferred. *Mihalov and Barnes* [1982] suggested that the mean ion escape rate was, however, much smaller. The ultimate source of the observed $O^+$ ions was unknown, but was suggested to include pickup ions, plasma clouds, or upward flow in holes.

[63] Using PV Orbiter Magnetometer (OMAG) data of the average properties of the magnetic field 8–10 $R_V$ down the wake, *McComas et al.* [1986] derived an average ion loss down the magnetotail of $10^{26}$ amu $s^{-1}$ or $6 \times 10^{24}$ $O^+$ $s^{-1}$. If all the ions are assumed to be $O^+$ of planetary origin, this represents a maximum hemispheric average flux of $2.7 \times 10^6$ $cm^{-2}$ $s^{-1}$.

### 7.4. VEX Observations of Escaping Ions

[64] The Venus Express (VEX) spacecraft, which is currently orbiting Venus, carries a plasma package that includes an ion mass analyzer, an electron spectrometer, and energetic neutral atoms imagers. *Barabash et al.* [2007] have reported VEX measurements that showed that dominant ions escaping are $O^+$ $He^+$, and $H^+$ in the plasma wake. The observed ratio $H^+$ to $O^+$ was 1.9, and that of $He^+$ to $O^+$ was 0.07. They suggested that the similarity of the spatial distributions of these particles confirms their ionospheric origin. There is not yet, however, enough spatial coverage to determine total ion escape rates, although Barabash et al. estimate a lower limit to the escape rate for $H^+$ of $10^{25}$ $s^{-1}$, equivalent to a hemispheric flux of $\sim 4 \times 10^6$, through the plasma wake. VEX has explored the Venus ionosphere at low solar activity, however, but further measurements at higher solar activity are expected.

## 8. Summary

[65] The nightside ionosphere of Venus is mostly formed by day-to-night transport of ions, which have been observed to flow upward and nightward, with a small contribution due to energetic electron precipitation from the wake region (see, e.g., the review by *Fox and Kliore* [1997]). Such fluxes of ions should produce ionospheres with an eroded appearance, in which the total ion or electron density scale heights are depressed compared to the ionospheres which are not subject to outward/horizontal flows. We have modeled the dayside ionosphere of Venus for various upward velocity boundary conditions imposed at the tops of the dayside models in order to determine both the maximum possible values of the upward fluxes, and the upward fluxes implied by comparison to PV data from three instruments, the ORO, the ORPA, and the OETP.

[66] We have constructed more than 60 models for solar maximum conditions and a SZA of 60°, with upward velocity boundary conditions in the range from 0 to $3 \times 10^5$ $cm^{-2}$. We present the ion and electron density profiles for four values of the upward velocities: 0, $2 \times 10^4$, $1 \times 10^5$, and $2 \times 10^5$ $cm^{-2}$ $s^{-1}$. It is apparent that as the upward velocity is increased the densities of the atomic ions decrease, as do the total ion and electron densities. The densities of the molecular ions, however, are observed to increase at high altitudes. We attribute this to the decrease in ambient electron densities, which leads to smaller molecular ion loss rates due to dissociative recombination.

[67] The maximum upward flux that we derive for an upward velocity of $3 \times 10^5$ $cm^{-2}$, is about $5.6 \times 10^8$ $cm^{-2}$ $s^{-1}$ for atomic ions, which are composed mostly of $O^+$. The maximum fluxes are source limited, and are determined roughly by the production rate of ions above the PCE boundary [*Fox*, 1997]. As the upward velocities increase, the PCE boundary is depressed at rates that are large at first and then smaller for velocities greater that $1 \times 10^5$ cm $s^{-1}$. The reduction in altitude of the PCE boundary increases the source region for the ions.

[68] By comparing our model profiles to those from PV data, we have derived the implied fluxes of $O^+$ that range from $1.8 \times 10^8$ to $2.5 \times 10^8$ $cm^{-2}$ $s^{-1}$. We have found an average value of $(2.1 \pm 0.4) \times 10^8$ $cm^{-2}$ $s^{-1}$, with an estimated accuracy of about 35%. The implied upward flux is roughly equal to estimates of the transterminator flux, of the total recombination rate of molecular ions over the nightside, and of the downward fluxes of ions over the nightside. From this, we infer that the escape flux due to ion outflow ranges from negligible to a maximum of about $(4–5) \times 10^7$ $cm^{-2}$ $s^{-1}$, which is equivalent to a total loss rate of $\sim 1 \times 10^{26}$ $s^{-1}$.

[69] We also review here estimates of the escape rate of ions from Venus due to various mechanisms, including pickup ion escape, which is fundamentally different from escape processes which have their origin in day-to-night ion flow. Pickup ion escape does not depress the scale heights of the ionosphere. We also discuss several mechanisms that could arise from the day-to-night flow of ions. In general, these predicted escape rates vary widely, and there is no general consensus about acceleration processes or the escape rates due to most of the mechanisms.

[70] Although the escape of ions from Venus appears not to be well constrained, the current estimated values of the escape fluxes are less than and sometimes much less than the estimated day-to-night fluxes of ions. Thus we conclude that the upward ion fluxes inferred by a comparison of the measurements of the dayside morphology of the ionosphere to our model ionospheres are indicative of the magnitude of the day-to-night flows. These fluxes, which are inferred to be much less than their maximum (source-limited) values,

probably contribute mostly to the formation of the nightside ionosphere, with only a small amount possibly contributing to escape.

[71] **Acknowledgments.** This work has been supported by NASA grant NNG06GF21G to Wright State University. The Solar2000 research grade irradiances are provided courtesy of W. Kent Tobiska and http://www.SpaceWx.com. These historical irradiances have been developed with funding from the NASA UARS, TIMED, and SOHO missions.

## References

Amerstorfer, U. V., N. V. Erkaev, D. Langmayr, and H. K. Biernat (2007), On Kelvin-Helmholtz instability due to the solar wind interaction with unmagnetized planets, *Planet. Space Sci.*, *55*, 1811–1816.

Ayres, T. (1997), Evolution of the solar ionizing flux, *J. Geophys. Res.*, *102*, 1641–1651.

Barabash, S., et al. (2007), The loss of ions from Venus through the plasma wake, *Nature*, *450*, 650–653, doi:10.1038/nature06434.

Biernat, H. K., N. V. Erkaev, U. V. Amerstorfer, T. Penz, and H. I. M. Lichtenegger (2007), Solar wind flow past Venus and its implications for the occurrence of the Kelvin-Helmholtz instability, *Planet. Space Sci.*, *55*, 1793–1803.

Brace, L. H., R. F. Theis, W. R. Hoegy, J. H. Wolfe, J. D. Mihalov, C. T. Russell, R. C. Elphic, and A. F. Nagy (1980), The dynamic behavior of the Venus ionosphere in response to solar wind interactions, *J. Geophys. Res.*, *85*, 7663–7678.

Brace, L. H., R. F. Theis, and W. R. Hoegy (1982a), Plasma clouds above the ionopause of Venus and their implications, *Planet. Space Sci.*, *30*, 29–37.

Brace, L. H., R. F. Theis, H. G. Mayr, S. A. Curtis, and J. G. Luhmann (1982b), Holes in the nightside ionosphere of Venus, *J. Geophys. Res.*, *87*, 199–211.

Brace, L. H., W. T. Kasprzak, H. A. Taylor, R. F. Theis, C. T. Russell, A. Barnes, J. D. Mihalov, and D. M. Hunten (1987), The ionotail of Venus: Its configuration and evidence for ion escape, *J. Geophys. Res.*, *92*, 15–26.

Brace, L. H., R. E. Hartle, and R. F. Theis (1995), The nightward ion flow scenario at Venus revisited, *Adv. Space Res.*, *16*, 99–112.

Brannon, J. F., and J. L. Fox (1994), The downward flux of $O^+$ over the nightside of Venus, *Icarus*, *112*, 396–404.

Brannon, J. F., J. L. Fox, and H. S. Porter (1993), Evidence for day-to-night transport at low solar activity in the Venus pre-dawn ionosphere, *Geophys. Res. Lett.*, *20*, 2739–2742.

Breus, T. K., K. I. Gringauz, and M. I. Verigin (1985), On the properties and origin of the Venus nightside ionosphere, *Adv. Space Res.*, *5*, 145–156.

Brinton, H. C., H. A. Taylor, H. B. Niemann, H. G. Mayr, A. F. Nagy, T. E. Cravens, and D. F. Strobel (1980), Venus nighttime hydrogen bulge, *Geophys. Res. Lett.*, *7*, 865–868.

Chen, R. H., T. E. Cravens, and A. F. Nagy (1978), The Martian ionosphere in light of the Viking observations, *J. Geophys. Res.*, *83*, 3871–3876.

Cravens, T. E., S. L. Crawford, A. F. Nagy, and T. Gombosi (1983), A two-dimensional model of the ionosphere of Venus, *J. Geophys. Res.*, *88*, 5595–5606.

Dobe, Z., A. F. Nagy, and J. L. Fox (1995), A theoretical study concerning the solar cycle dependence of the nightside ionosphere of Venus, *J. Geophys. Res.*, *100*, 14,507–14,513.

Donahue, T. M., and R. E. Hartle (1992), Solar cycle variations in $H^+$ and $D^+$ densities in the Venus ionosphere: Implications for escape, *Geophys. Res. Lett.*, *19*, 2449–2452.

Fox, J. L. (1992), The chemistry of the nightside ionosphere of Venus, *Planet. Space Sci.*, *40*, 1663–1668.

Fox, J. L. (1993), The production and escape of nitrogen atoms on Mars, *J. Geophys. Res.*, *98*, 3297–3310.

Fox, J. L. (1997), Upper limits to the outflow of ions at Mars: Implications for atmospheric evolution, *Geophys. Res. Lett.*, *24*, 2901–2904.

Fox, J. L. (2003), The effect of $H_2$ on the Martian ionosphere: Implications for atmospheric evolution, *J. Geophys. Res.*, *108*(A6), 1223, doi:10.1029/2001JA000203.

Fox, J. L. (2004), Response of the Martian thermosphere/ionosphere to enhanced fluxes of solar soft X rays, *J. Geophys. Res.*, *109*, A11310, doi:10.1029/2004JA010380.

Fox, J. L. (2007), Near-terminator Venus ionosphere: How Chapman-esque?, *J. Geophys. Res.*, *112*, E04S02, doi:10.1029/2006JE002736.

Fox, J. L., and A. J. Kliore (1997), Ionosphere: Solar activity variations, in *Venus II*, edited by S. Bougher et al., pp. 161–188, Univ. of Ariz. Press, Tucson.

Fox, J. L., and A. I. F. Stewart (1991), The Venus ultraviolet aurora: A soft electron source, *J. Geophys. Res.*, *96*, 9821–9828.

Fox, J. L., and K. Y. Sung (2001), Solar activity variations in the Venus ionosphere/thermosphere, *J. Geophys. Res.*, *106*, 21,305–21,335.

Fox, J. L., and K. E. Yeager (2006), Morphology of the near-terminator Martian ionosphere: A comparison of models and data, *J. Geophys. Res.*, *111*, A10309, doi:10.1029/2006JA011697.

Fox, J. L., J. F. Brannon, A. I. F. Stewart, and H. S. Porter (1992), Model calculations of the nightside ionospheres of Venus and Mars, *Bull. Am. Astron. Soc.*, *24*, 997.

Froese-Fischer, C., and G. Tachiev (2004), Breit-Pauli energy levels, lifetimes, and transition probabilities for the beryllium-like to neon-like sequences, *At. Data. Nucl. Data Tables*, *87*, 1–184.

Grebowsky, J. M., and S. A. Curtis (1981), Venus nightside ionospheric holes: The signatures of parallel electric field acceleration regions?, *Geophys. Res. Lett.*, *8*, 1273–1276.

Grebowsky, J. M., W. T. Kasprzak, R. E. Hartle, and T. M. Donahue (1995), A new look at Venus thermosphere H distribution, *Adv. Space Res.*, *17*, 191–195.

Gringauz, K. I., M. I. Verigin, T. K. Breus, and T. Gombosi (1977), Electron currents measured in the optical shadow of Venus by the "Venera-9" and "Venera-10" satellites: The basic source of ionization in the nighttime ionosphere of Venus, *Sov. Phys. Dokl.*, Engl. Transl., *22*, 53–56.

Gringauz, K. I., M. I. Verigin, T. K. Breus, and T. Gombosi (1979), The interaction of electrons in the optical umbra of Venus with the planetary atmosphere: The origin of the nighttime ionosphere, *J. Geophys. Res.*, *84*, 2123–2127.

Hartle, R. E., and J. M. Grebowsky (1990), Upward ion flow in ionospheric holes on Venus, *J. Geophys. Res.*, *95*, 31–37.

Hartle, R. E., and J. M. Grebowsky (1993), Light ion flow in the nightside ionosphere of Venus, *J. Geophys. Res.*, *98*, 7437–7445.

Hartle, R. E., and J. M. Grebowsky (1995), Planetary loss from light ion escape on Venus, *Adv. Space Res.*, *15*, 117–122.

Hedin, A. E., H. B. Niemann, W. T. Kasprzak, and A. Seiff (1983), Global empirical model of the Venus thermosphere, *J. Geophys. Res.*, *88*, 73–83.

Hinteregger, H. E., K. Fukui, and B. R. Gibson (1981), Observational, reference and model data on solar EUV, from measurements on AE-E, *Geophys. Res. Lett.*, *8*, 1147–1150.

Intriligator, D. S. (1989), Results of the first statistical study of Pioneer Venus Orbiter plasma observations in the distant Venus tail: Evidence for a hemispheric asymmetry in the pickup of ionospheric ions, *Geophys. Res. Lett.*, *16*, 167–170.

Kallio, E., R. Jarvinen, and P. Janhunen (2006), Venus-solar wind interaction: Asymmetries and the escape of $O^+$ ions, *Planet. Space Sci.*, *54*, 1472–1481.

Kasprzak, W. T., H. B. Niemann, and P. Mahaffy (1987), Observations of energetic ions on the nightside of Venus, *J. Geophys. Res.*, *92*, 291–298.

Kasprzak, W. T., J. M. Grebowsky, H. B. Niemann, and L. H. Brace (1991), Superthermal >36-eV ions observed in the near-terminator region of Venus by the Pioneer Venus Orbiter Neutral Mass Spectrometer, *J. Geophys. Res.*, *96*, 11,175–11,187.

Kliore, A. J. (1992), Radio occultation observations of the ionospheres of Venus and Mars, in *Venus and Mars: Atmospheres, Ionospheres and Solar Wind Interaction*, *Geophys. Monogr. Ser.*, vol. 66, edited by J. G. Luhmann, M. Tatrallyay, and R. Pepin, pp. 265–276, AGU, Washington, D. C.

Kliore, A. J., and J. G. Luhmann (1991), Solar cycle effects on the structure of the electron density profiles in the dayside ionosphere of Venus, *J. Geophys. Res.*, *96*, 21,281–21,289.

Kliore, A. J., and L. F. Mullen (1989), Long-term behavior of the main peak of the dayside ionosphere of Venus during solar cycle 21 and its implications on the effect of the solar cycle upon the electron temperature in the main peak region, *J. Geophys. Res.*, *94*, 13,339–13,351.

Kliore, A. J., G. S. Levy, D. L. Cain, G. Fjeldbo, and S. I. Rasool (1967), Atmosphere and ionosphere of Venus from the Mariner 5 S-band radio occultation measurements, *Science*, *158*, 1683–1688.

Kliore, A. J., I. R. Patel, A. F. Nagy, T. E. Cravens, and T. I. Gombosi (1979), Initial observations of the nightside ionosphere of Venus from Pioneer-Venus orbiter occultation measurements, *Science*, *205*, 99–102.

Kliore, A. J., J. G. Luhmann, and M. H. G. Zhang (1991), The effect of the solar cycle on the maintenance of the nightside ionosphere of Venus, *J. Geophys. Res.*, *96*, 11,065–11,071.

Knudsen, W. C. (1992), The Venus ionosphere from in situ measurements, in *Venus and Mars: Atmospheres Ionospheres and Solar Wind Interactions*, *Geophys. Monogr. Ser.*, vol. 66, edited by J. G. Luhmann, M. Tatrallyay, and R. Pepin, pp. 237–263, AGU, Washington, D. C.

Knudsen, W. C., and K. L. Miller (1985), Pioneer Venus suprathermal electron flux measurements in the Venus umbra, *J. Geophys. Res.*, *90*, 2697–2702.

Knudsen, W. C., and K. L. Miller (1992), The Venus transterminator ion flux at solar maximum, *J. Geophys. Res.*, *97*, 17,165–17,167.

Knudsen, W. C., K. Spenner, K. L. Miller, and V. Novak (1980a), Transport of ionospheric $O^+$ ions across the Venus terminator and implications, *J. Geophys. Res.*, *85*, 7803–7810.

Knudsen, W. C., K. Spenner, P. F. Michaelson, R. C. Whitten, K. L. Miller, and V. Novak (1980b), Suprathermal electron energy distribution within the dayside Venus ionosphere, *J. Geophys. Res.*, *85*, 7754–7758.

Knudsen, W. C., K. Spenner, and K. L. Miller (1981), Anti-solar acceleration of ionospheric plasma across the Venus terminator, *Geophys. Res. Lett.*, *8*, 281–284.

Kulikov, Y. N., et al. (2006), Atmospheric and water loss from early Venus, *Planet. Space Sci.*, *54*, 142–1444.

Lammer, H., et al. (2006), Loss of hydrogen and oxygen from the upper atmosphere of Venus, *Planet. Space Sci.*, *54*, 1445–1456.

Luhmann, J. G., and S. J. Bauer (1992), Solar wind effects on atmospheric evolution at Venus and Mars, in *Venus and Mars: Atmospheres, Ionospheres and Solar Wind Interaction*, *Geophys. Monogr. Ser.*, vol. 66, edited by J. G. Luhmann, M. Tatrallyay, and R. Pepin, pp. 417–430, AGU, Washington, D. C.

Luhmann, J. G., R. E. Johnson, and M. H. G. Zhang (1992), Evolutionary impact of sputtering of the Martian atmosphere by $O^+$ pickup ions, *Geophys. Res. Lett.*, *19*, 2151–2154.

Luhmann, J. G., W. T. Kasprzak, and J. M. Grebowsky (1995), On removing molecular ions from Venus, *J. Geophys. Res.*, *100*, 14,515–14,521.

Luhmann, J. G., W. T. Kasprzak, and C. T. Russell (2007), Space weather at Venus and its potential consequences for atmospheric evolution, *J. Geophys. Res.*, *112*, E04S10, doi:10.1029/2006JE002820.

Mariner Stanford Group (1967), Venus: Ionosphere and atmosphere as measured by dual-frequency radio occultation of Mariner V, *Science*, *158*, 1678–1683.

McComas, D. J., H. E. Spence, C. T. Russell, and M. A. Saunders (1986), The average magnetic field draping and consistent plasma properties of the Venus magnetotail, *J. Geophys. Res.*, *91*, 7939–7953.

McElroy, M. B., and D. F. Strobel (1969), Models for the Venus nightside ionosphere, *J. Geophys. Res.*, *74*, 1118–1127.

Mihalov, J. D., and A. Barnes (1982), The distant interplanetary wake of Venus: Plasma observations from Pioneer Venus, *J. Geophys. Res.*, *87*, 9045–9053.

Mihalov, J. D., J. H. Wolfe, and D. S. Intriligator (1980), Pioneer Venus plasma observations of the solar wind-Venus interaction, *J. Geophys. Res.*, *85*, 7613–7624.

Miller, K. L., and R. C. Whitten (1991), Ion dynamics in the Venus ionosphere, *Space Sci. Rev.*, *55*, 165–199.

Miller, K. L., W. C. Knudsen, K. Spenner, R. C. Whitten, and V. Novak (1980), Solar zenith angle dependence of ionospheric ion and electron temperatures and densities on Venus, *J. Geophys. Res.*, *85*, 7759–7764.

Miller, K. L., W. C. Knudsen, and K. Spenner (1984), The dayside Venus ionosphere: I. Pioneer-Venus retarding potential analyzer experimental observations, *Icarus*, *57*, 386–409.

Nagy, A. F., A. Körösmezey, J. Kim, and T. I. Gombosi (1991), A two dimensional shock capturing hydrodynamic model of the Venus ionosphere, *Geophys. Res. Lett.*, *18*, 801–804.

Niemann, H. B., W. T. Kasprzak, A. E. Hedin, D. M. Hunten, and N. W. Spencer (1980), Mass spectrometric measurements of the neutral gas composition of the thermosphere and exosphere of Venus, *J. Geophys. Res.*, *85*, 7817–7828.

Pérez-de-Tejada, H. (1980), Evidence for a viscous boundary layer at the Venus ionopause from the preliminary Pioneer Venus results, *J. Geophys. Res.*, *85*, 7709–7714.

Shinagawa, H., and T. E. Cravens (1989), A one-dimensional multispecies magnetohydrodynamic model of the dayside ionosphere of Mars, *J. Geophys. Res.*, *94*, 6506–6516.

Spenner, K., W. C. Knudsen, R. C. Whitten, P. F. Michaelson, K. L. Miller, and V. Novak (1981), On the maintenance of the Venus nightside ionosphere: Electron precipitation and plasma transport, *J. Geophys. Res.*, *86*, 9170–9178.

Spenner, K., W. C. Knudsen, and W. Lotze (1996), Suprathermal electron fluxes in the Venus ionosphere at moderate and high solar activities, *J. Geophys. Res.*, *101*, 4557–4563.

Taylor, H. A., H. C. Brinton, S. J. Bauer, R. E. Hartle, P. A. Cloutier, and R. E. Daniell (1980), Global observations of the composition and dynamics of the ionosphere of Venus: Implications for the solar wind interaction, *J. Geophys. Res.*, *85*, 7765–7777.

Taylor, H. A., H. C. Brinton, H. B. Niemann, H. G. Mayr, R. E. Hartle, A. Barnes, and J. Larson (1984), Interannual and short-term variations of the Venus nighttime hydrogen bulge, *J. Geophys. Res.*, *89*, 10,669–10,675.

Taylor, H. A., H. C. Brinton, H. B. Niemann, H. G. Mayr, R. E. Hartle, A. Barnes, and J. Larson (1985), In situ results on the variation of neutral atmospheric hydrogen at Venus, *Adv. Space Res.*, *5*, 125–128.

Terada, N., S. Machida, and H. Shinagawa (2002), Global hybrid simulation of the Kelvin-Helmholtz instability at the Venus ionopause, *J. Geophys. Res.*, *107*(A12), 1471, doi:10.1029/2001JA009224.

Terada, N., H. Shinagawa, and S. Machida (2004), Global hybrid model of the solar wind interaction with the Venus ionosphere: Ion escape processes, *Adv. Space Res.*, *33*, 161–166.

Theis, R. F., L. H. Brace, and H. G. Mayr (1980), Empirical models of the electron temperature and density in the Venus ionosphere, *J. Geophys. Res.*, *85*, 7787–7794.

Theis, R. F., L. H. Brace, R. C. Elphic, and H. G. Mayr (1984), New empirical models of the electron temperature and density in the Venus ionosphere with application to transterminator flow, *J. Geophys. Res.*, *89*, 1477–1488.

Tobiska, W. K. (2004), SOLAR2000 irradiances for climate change, aeronomy and space system engineering, *Adv. Space Res.*, *34*, 1736–1746.

Whitten, R. C., B. Baldwin, W. C. Knudsen, K. L. Miller, and K. Spenner (1982), The Venus ionosphere at grazing incidence of solar radiation: Transport of plasma to the night ionosphere, *Icarus*, *51*, 261–270.

Whitten, R. C., P. T. McCormick, D. Merritt, K. W. Thompson, R. R. Brynsvold, C. J. Eich, W. C. Knudsen, and K. L. Miller (1984), Dynamics of the Venus ionosphere: A two-dimensional model study, *Icarus*, *60*, 317–326.

Woods, T. N., F. G. Eparvier, S. M. Bailey, P. C. Charberlin, J. Lean, G. J. Rottman, S. C. Solomon, W. K. Tobiska, and D. L. Woodraska (2005), Solar EUV Experiment (SEE): Mission overview and first results, *J. Geophys. Res.*, *110*, A01312, doi:10.1029/2004JA010765.

J. L. Fox, Department of Physics, Wright State University, 3640 Colonel Glenn Highway, Dayton, OH 45435, USA. (jane.fox@wright.edu)